Sankar, S. S., La Mar, G. N., Smith, K. M., & Fujinari, E. M. (1987) *Biochim. Biophys. Acta 912*, 220-229.
Satterlee, J. D. (1985) *Annu. Rep. NMR Spectrosc. 17*, 79-178.
Shulman, R. G., Glarum, S. H., & Karplus, M. (1971) *J. Mol. Biol. 57*, 93-115.
Springer, B. A., Egeberg, K. D., Sligar, S. G., Rohlfs, J. M., & Olson, J. S. (1989) *J. Biol Chem. 264*, 3057-3060.
States, D. J., Haberkorn, R. A., & Ruben, D. J. (1982) *J. Magn. Reson. 48*, 286-292.
Swift, T. J. (1973) in *NMR of Paramagnetic Molecules* (La Mar, G. N., Horrocks, W. D., Jr., & Holm, R. H., Eds.) pp 53-83, Academic Press, New York.
Takano, T. (1977) *J. Mol. Biol. 110*, 537-568.
Thanabal, V., de Ropp, J. S., & La Mar, G. N. (1987a) *J. Am. Chem. Soc. 109*, 265-272.
Thanabal, V., de Ropp, J. S., & La Mar, G. N. (1987b) *J. Am. Chem. Soc. 109*, 7516-7525.
Thanabal, V., de Ropp, J. S., & La Mar, G. N. (1988) *J. Am. Chem. Soc. 110*, 3027-3035.
Unger, S. W., Jue, T., & La Mar, G. N. (1985) *J. Magn. Reson. 61*, 448-456.
Williams, G., Moore, G. R., Porteous, R., Robinson, M. N., Soffe, N., & Williams, R. J. P. (1985a) *J. Mol. Biol. 183*, 409-428.
Williams, G., Clayden, N. J., Moore, G. R., & Williams, R. J. P. (1985b) *J. Mol. Biol. 183*, 447-460.
Wüthrich, K. (1986) *NMR of Proteins and Nucleic Acids*, Wiley, New York.
Wüthrich, K., Shulman, R. G., Yamane, T., Wyluda, B. J., Hügli, T. E., & Gurd, F. R. N. (1970) *J. Biol. Chem. 245*, 1947-1953.

NMR Determination of the Orientation of the Magnetic Susceptibility Tensor in Cyanometmyoglobin: A New Probe of Steric Tilt of Bound Ligand†

S. Donald Emerson and Gerd N. La Mar*
Department of Chemistry, University of California, Davis, California 95616
Received June 6, 1989; Revised Manuscript Received September 11, 1989

ABSTRACT: The experimentally determined paramagnetic dipolar shifts for noncoordinated amino acid side-chain protons in the heme pocket of sperm whale cyanometmyoglobin [Emerson, S. D., & La Mar, G. N. (1990) *Biochemistry* (preceding paper in this issue)] were used to determine in solution the orientation of the principal axes for the paramagnetic susceptibility tensor relative to the heme iron molecular coordinates. The determination was made by a least-squares search for the unique Euler rotation angles which convert the geometric factors in the molecular (crystal) coordinates to ones that correctly predict each of 41 known dipolar shifts by using the magnetic anisotropies computed previously [Horrocks, W. D., Jr., & Greenberg, E. S. (1973) *Biochim. Biophys. Acta 322*, 38-44]. An excellent fit to experimental shifts was obtained, which also provided predictions that allowed subsequent new assignments to be made. The magnetic axes are oriented so that the z axis is tipped $\sim 15°$ from the heme normal toward the heme δ-meso-H and coincides approximately with the characterized FeCO tilt axis in the isostructural MbCO complex [Kuriyan, J., Wilz, S., Karplus, M., & Petsko, G. A. (1986) *J. Mol. Biol. 192*, 133-154]. Since the FeCO and FeCN units are isostructural, we propose that the dominant protein constraint that tips the magnetic z axis from the heme normal is the tilt of the FeCN by steric interactions with the distal residues. The rhombic magnetic axes were found to align closely with the projection of the proximal His imidazole plane on the heme, confirming that the His-Fe bonding provides the protein constraint that orients the in-plane anisotropy. The tipped magnetic z axis is shown to account quantitatively for the previously noted major discrepancy between the hyperfine shift patterns for the bound imidazole side chain in models and protein. Moreover, it is shown that the proximal His ring nonlabile proton hyperfine shifts provide direct and exquisitely sensitive indicators of the degree of the z axis tilt that may serve as a valuable probe for characterizing variable steric interactions in the distal pocket of both point mutants and natural genetic variants of myoglobin.

The inherently high information content of the hyperfine-shifted resonances of low-spin ferric hemoproteins has long been recognized, and extensive NMR studies of both model compounds and various hemoproteins have been reported (Wüthrich, 1970; Shulman et al., 1971; La Mar, 1979; La Mar & Walker, 1979; Satterlee, 1985). These hyperfine shift patterns are highly sensitive to systematic perturbations as found in closely related natural genetic variants and synthetic point mutants of myoglobin (Mb)[1] and contain key information on the modulation of chemical reactivity by the nature of the polypeptide chain (Wüthrich et al., 1970; Krishnamoorthi et al., 1984; Satterlee, 1985; Springer et al., 1989). The full exploitation of this information, however, has to date been prevented because of the inability to unambiguously assign the heme pocket residue peaks and to quantitatively separate the dipolar and contact contributions to the observed hyperfine shift (Jesson, 1973; Horrocks, 1973; Bertini & Luchinat, 1986):

$$\delta_{hf} = \delta_{con} + \delta_{dip} \quad (1)$$

† This research has been supported by a grant from the National Institutes of Health (HL 16087).

[1] Abbreviations: Mb, myoglobin; Hb, hemoglobin; metMbCN, cyanide-complexed ferric Mb; NMR, nuclear magnetic resonance; DSS, 2,2-dimethyl-2-silapentane-5-sulfonate; ESR, electron spin resonance.

0006-2960/90/0429-1556$02.50/0

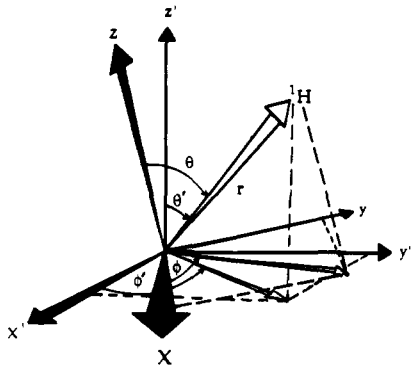

FIGURE 1: Coordinate systems describing the magnetic axes (x,y,z or r,θ,ϕ) in which the magnetic susceptibility tensor is diagonal and in which geometric factors must be calculated, and the iron-centered pseudosymmetry coordinates (x',y',z' or r',θ',ϕ') obtainable from available crystal coordintes of MbCO. The two coordinate systems are related by $[x,y,z] = [x',y',z']R(\alpha,\beta,\gamma)$, where α,β,γ are the three angles of the standard Eulerian transformation (Arfkin, 1985).

In our companion report, we have secured the needed majority of the resonance assignments for residues in the heme pocket of the cyanide-ligated ferric sperm whale myoglobin complex, metMbCN, using one- and two-dimensional NMR methodologies together with paramagnetic-induced relaxation (Emerson & La Mar, 1990). Here we consider a method for quantitatively separating the contact and dipolar shift, which has as its basis the quantitative calculation of the dipolar shifts as given by (Jesson, 1973)

$$\delta_{dip}(\text{calc}) = -\frac{\Delta\chi_{ax}}{3N}F_{ax}(r,\theta,\phi) - \frac{\Delta\chi_{rh}}{2N}F_{rh}(r,\theta,\phi) \quad (2)$$

with the axial and rhombic magnetic anisotropies

$$\Delta\chi_{ax} = \chi_{zz} - \tfrac{1}{2}(\chi_{xx} + \chi_{yy}) \qquad \Delta\chi_{rh} = \chi_{xx} - \chi_{yy} \quad (3)$$

Avogadro's number N, and the axial and rhombic geometric factors

$$F_{ax} = (3\cos^2\theta - 1)r^{-3} \qquad F_{rh} = (\sin^2\theta\cos 2\phi)r^{-3} \quad (4)$$

where χ_{ii} are the principal components of the diagonal magnetic susceptibility tensor, χ, and r,θ,ϕ (or x,y,z) are the *polar (Cartesian) coordinates of the proton of interest within the coordinate system in which χ is diagonal*, i.e., the x, y, z system in Figure 1.

The components of the diagonal susceptibility tensor have not been experimentally determined but have been adequately estimated (Horrocks & Greenberg, 1973) on the basis of the low-temperature g values of the lowest Kramers doublet (Hori, 1971) using ligand field theory that includes both first-order and second-order Zeeman interactions. The position vectors for protons in metMbCN are most readily available in the molecular coordinate system, x',y',z' (or r,θ',ϕ'), as provided by the X-ray structure of isostructural MbCO (Kuriyan et al., 1986). The problem then reduces to identifying the Eulerian rotation matrix, $R(\alpha,\beta,\gamma)$, which converts $(x',y',z') \xrightarrow{R(\alpha,\beta,\gamma)} (x,y,z)$, or $(r,\theta',\phi') \xrightarrow{R(\alpha,\beta,\gamma)} (r,\theta,\phi)$ in Figure 1 (Arfkin, 1985). This allows us to recast eq 2 in terms of geometric factors in the pseudosymmetry X-ray coordinate based system, r,θ',ϕ':

$$\delta_{dip}(\text{calc}) = \delta'_{dip}(\text{calc})R(\alpha,\beta,\gamma) = -\left[\frac{\Delta\chi_{ax}}{3N}F_{ax}(r,\theta',\phi') + \frac{\Delta\chi_{rh}}{2N}F_{rh}(r,\theta',\phi')\right]R(\alpha,\beta,\gamma) \quad (5)$$

where $\delta'_{dip}(\text{calc})$ and $\delta_{dip}(\text{calc})$ are computed in the molecular (r,θ',ϕ') and magnetic (r,θ,ϕ) coordinate systems, respectively.

Two different magnetic coordinate systems have been proposed (shown in part A of Figure 2) on the basis of low-temperature ESR studies on single crystals (Hori, 1971; Peisach et al., 1971). However, a plot of the observed versus calculated δ_{dip} using these coordinate systems fails to show satisfactory correlation, as shown in parts A and B of Figure 3, with numerous peaks displaying dipolar shifts of the wrong sign (see below). The lack of a quantitative correlation between $\delta_{dip}(\text{obs})$ and $\delta_{dip}(\text{calc})$, and in particular, the failure to predict the correct sign of δ_{dip} in numerous cases, indicates that the low-temperature single-crystal magnetic axes do not describe the ambient temperature solution system. The location of the magnetic axes in sperm whale metMbCN at ambient temperature can be expected to shed light on the nature of the heme–protein contacts that are the determinants of the magnetic axes (Shulman et al., 1971; Traylor & Berzinis, 1980). In turn, these orientations could serve as valuable probes for assessing molecular and/or electronic perturbation characteristics of either natural genetic variants or synthetic point mutants of myoglobin.

We determine here experimentally $R(\alpha,\beta,\gamma)$ via solution ^{1}H NMR by carrying out a computer least-squares search for the rotation angles, α,β,γ, which quantitatively predicts via eq 5 all experimentally determined dipolar shifts for noncoordinated amino acid side-chain protons of metMbCN. Of interest are answers to the following questions: Can a unique orientation

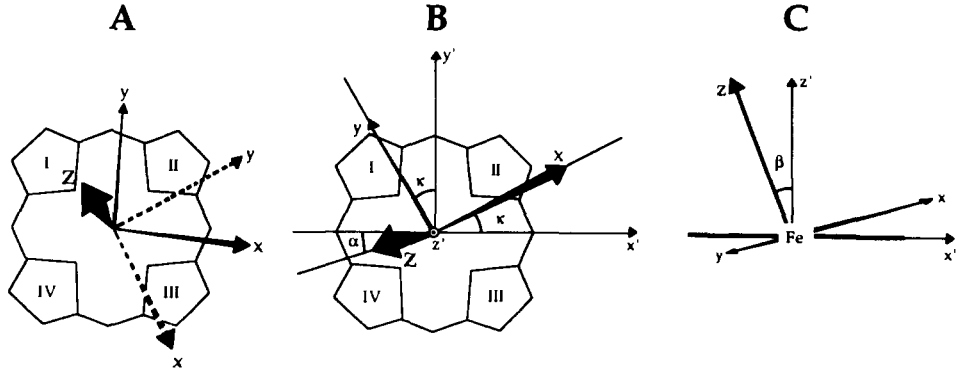

FIGURE 2: Various magnetic axes used to describe the dipolar shifts for sperm whale metMbCN. In all cases, the symmetry axes derived from MbCO X-ray data have x',y' intersecting the meso positions. (A) As determined by Hori (1971) from low-temperature single-crystal ESR data (solid lines; $\alpha = -57.5°$, $\beta = -13°$, $\gamma = 44.8°$), and as proposed by Peisach et al. (1971) (dotted lines; $\alpha = -57.5°$, $\beta = -13°$, $\gamma = 0.0°$): they share the same z axis tilted 13° toward the 2-vinyl position. (B) Face-on view and (C) edge-on view of the magnetic coordinate system determined by computer least-squares fit minimizing differences between observed and calculated dipolar shifts (eq 8). The z axis was invariably tilted ~15° in the direction of the δ-meso position. The α of $R(\alpha,\beta,\gamma)$ is defined by the angle between the projection of z on the old x',y' (heme) plane (B), and β defines the tilt from the heme normal (C). For small β, the projection of the new x–y axes on the heme plane makes an angle κ with the x',y' axes given by $\kappa \sim \alpha + \gamma$.

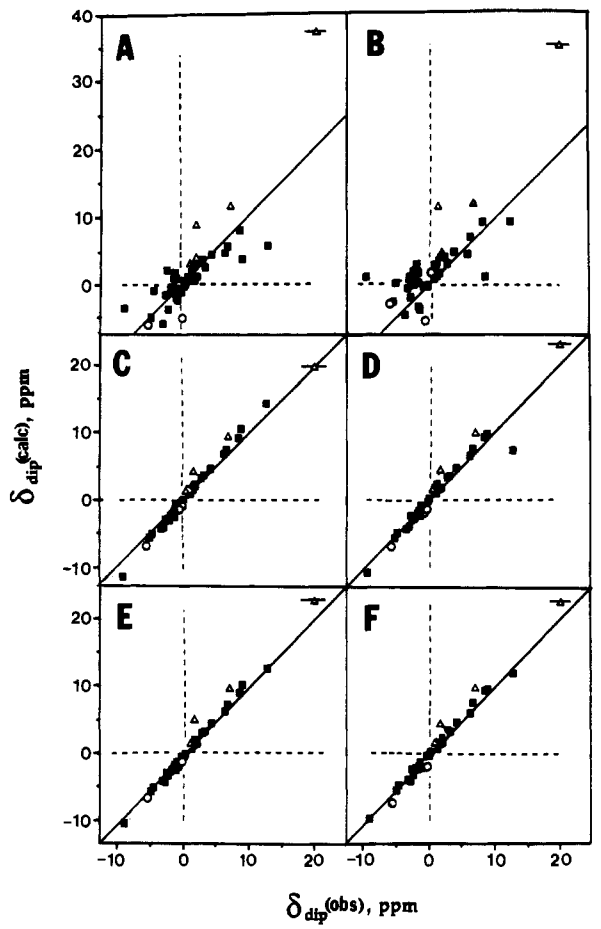

FIGURE 3: Plots of observed dipolar shift versus dipolar shifts calculated with eq 3 by using a variety of magnetic axes defined by $R(\alpha,\beta,\gamma)$ and the available components of the susceptibility tensor. The data points for His E7 are given as open triangles, and those of Val E11 as open circles; all other data points are given as solid squares. The His E7 $N_\epsilon H$ dipolar shift has a large (±3 ppm) uncertainty[2] due to the uncertain δ_{dia}. (A) Magnetic axes of Hori (1971) ($\alpha = -57.5°$, $\beta = -13°$, $\gamma = 44.8°$) with $\kappa = -13°$; $F/n = 8.1$ ppm^2, plotting points numbered 1–41 in Table I. (B) Magnetic axes of Peisach et al. (1971) ($\alpha = -57.5°$, $\beta = -13°$, $\gamma = 0°$) with $\kappa = -57°$; $F/n = 12$ ppm^2, plotting points 1–41 in Table I. (C) Magnetic axes ($\alpha = 0°$, $\beta = -14.0°$, $\gamma = 35°$, with $\kappa = 35°$) derived from minimizing F/n via eq 8 using all input data points 1–41 in Table I; $F/n = 0.98$ ppm^2. (D) Magnetic axes ($\alpha = 10°$, $\beta = -15.5°$, $\gamma = 20°$, $\kappa = 30°$) derived from minimizing F/n via eq 8 by excluding only His E7 signals from the input data (points 1–37 in Table I); $F/n = 0.71$ ppm^2. (E) Magnetic axes ($\alpha = 10°$, $\beta = -14.5°$, $\gamma = 25°$, $\kappa = 35°$) derived from minimizing F/n via eq 8 by excluding only Val E11 signals from the input data (points 1–33 and 38–41 in Table I); $F/n = 0.71$ ppm^2. (F) Magnetic axes ($\alpha = 0°$, $\beta = -14.5°$, $\gamma = 35°$, $\kappa = 35°$) derived from minimizing F/n via eq 8 by excluding both His E7 and Val E11 signals from the input data (points 1–33 in Table I); $F/n = 0.28$ ppm^2. For D–F, the data points for the two amino acid residues not used in the computer search, His E7 and/or Val E11, are also included for comparison.

of the magnetic axes for metMbCN be determined by solution NMR? What determines the location of its "in-plane" rhombic axes? What molecular deformation of the active site results in "tilting" of the z axis from the heme normal? Can the quantitative factoring of the dipolar and contact shifts shed light on the basis for the unprecedented discrepancy in the proximal histidine ring hyperfine shift pattern between model compounds and proteins, as found in our companion report (Emerson & La Mar, 1990)?

METHODS

Components of the Susceptibility Tensor. We use the values at 25 °C computed by Horrocks and Greenberg (1973) using ligand field theory, including both first- and second-order Zeeman terms, and based on the single-crystal g tensor as determined by Hori (1971). The values for the three components are $\chi_{xx} = 1263 \times 10^{-12}$ m^3/mol, $\chi_{yy} = 1836 \times 10^{-12}$ m^3/mol, and $\chi_{zz} = 3748 \times 10^{-12}$ m^3/mol at 25 °C, leading to $\Delta\chi_{ax} = 2198 \times 10^{-12}$ m^3/mol and $\Delta\chi_{rh} = -573 \times 10^{-12}$ m^3/mol for eq 3.

Hyperfine Shifts. The experimental shift is referenced to 2,2-dimethyl-2-propane-5-sulfonate (DSS), δ_{DSS}(obs), and is related to the hyperfine component (or solely dipolar component for noncoordinated residues) via (Jessson, 1973)

$$\delta_{DSS}(obs) = \delta_{hf} + \delta_{dia} \quad (6)$$

where δ_{dia} is the chemical shift (relative to DSS) for the same functional group in an isostructural diamagnetic system. We utilize here for δ_{dia} the observed shift as reported for the isostructural diamagnetic MbCO [δ_{dia}(MbCO)], where available (Mabbutt & Wright, 1985; Dalvit & Wright, 1987). In other cases, we use the conventional estimate:

$$\delta_{dia}(calc) = \delta_{tetra} + \delta_{rc} \quad (7)$$

where the former is the available tetrapeptide (Bundi & Wüthrich, 1979) shift and δ_{rc} is the ring current due to the heme and/or other aromatic side chain computed by using crystal coordinates and the eight-loop program of Cross and Wright (1985). The estimates using eq 7 should be valid to ±0.3 ppm. The differences in δ_{dia} using other ring current programs were small compared to the accuracy to which we can predict dipolar shifts and did not influence the determined orientation of the magnetic axes.

The input ^{1}H NMR data for obtaining the magnetic axes are the dipolar shifts for the signals of the noncoordinated residues assigned by 1D and 2D NMR methodology in our companion report (Emerson & La Mar, 1990). Since δ_{con} is likely nonzero for any iron-coordinated residue (La Mar, 1979; La Mar & Walker, 1979), we exclude both heme and His F8 shifts as input data. The δ_{DSS}(obs) yields δ_{dip}(obs) for noncoordinated residues by using eqs 6 and 7 and either δ_{dia}(MbCO) or δ_{dia}(calc). Input data were further restricted to those assigned peaks for which the variable-temperature slopes have been determined from 1D NOE experiments carried out in the range 5–40 °C; such peaks are numbered 1–41 in Table I [see also preceding paper (Emerson & La Mar, 1990)]. The shifts for signals assigned solely by 2D NOESY/COSY connectivities at 30 °C are extrapolated to 25 °C by using the straight line established from the plot of δ_{dip}(obs) versus slope for those signals for which both slope and shift data are available.

Search for Magnetic Axes. We define a normalized error function, $(1/n)F(\alpha,\beta,\gamma)$, as

$$(1/n)F(\alpha,\beta,\gamma) = \sum_{\substack{n \\ \text{assigned} \\ \text{noncoord} \\ \text{residue} \\ \text{signals}}} [\delta_{dip}(obs) - \delta'_{dip}(calc)R(\alpha,\beta,\gamma)]^2 \quad (8)$$

where δ'_{dip}(calc) is obtained in the pseudosymmetry crystal coordinate system, r,θ',ϕ', (i.e., x',y',z' in Figure 2), and $R(\alpha,\beta,\gamma)$ is the Eulerian rotation matrix (Arfkin, 1985) that converts the molecular pseudosymmetry coordinate system to the true magnetic axes. For methyl groups, $F(r,\theta',\phi')$ was averaged over complete rotation, and for the aromatic side chains known to reorient rapidly about their 2-fold axes on the NMR time scale (Dalvit & Wright, 1987; Emerson et al., 1988), the input δ_{dip}(calc) was averaged over the two crystallographically nonequivalent ring H_δs and H_ϵs. The Euler angles, α,β,γ, that minimize F/n define the principal coor-

Table I: Chemical Shift Data for Noncoordinated Heme Pocket Amino Acid Residues[a]

no.[b]	residue	position	δ_{DSS}(obs)[a,c]	δ_{dia}[a,d]	δ_{dip}(obs)[a,e]	δ_{dip}(calc)[a,f] axial	rhombic	total
g	Leu B10	$C_\gamma H$	3.96	0.86	3.10	2.98	0.11	3.10
1		$C_{\delta 1}H_3$	3.81	−0.26	4.07	4.78	0.00	4.78
2		$C_{\delta 2}H_3$	5.53	−0.67	6.20	6.07	0.14	6.21
3	Phe B14	$C_\delta Hs$	8.04	7.01	1.03	0.93	−0.09	0.84[k]
4		$C_\epsilon Hs$	8.37	6.45	1.92	1.87	−0.15	1.72[k]
5		$C_\zeta H$	8.40	5.22	3.18	3.49	−0.09	3.40
6	Phe CD1	$C_\delta Hs$	8.70	7.29	1.41	1.33	0.24	1.57[m]
7		$C_\epsilon Hs$	12.58	6.08	6.50	7.37	0.27	7.64[m]
8		$C_\zeta H$	17.27	4.72	12.55	13.54	−1.43	12.11
9	Phe CD4	$C_\delta Hs$	7.69	6.72	0.97	1.69	0.08	1.77[n]
10		$C_\epsilon Hs$	8.05	6.52	1.53	2.32	0.13	2.45[n]
11	Thr E10	$C_\alpha H$	2.50	3.83	−1.33	−1.02	−0.51	−1.53
12		$C_\beta H$	2.69	3.97	−1.28	−0.97	−0.95	−1.92
13		$C_\gamma H_3$	−1.56	1.51	−3.07	−2.78	−1.13	−3.91
g	Ala E14	$C_\alpha H$	3.46	4.63	−1.17	−1.06	−0.22	−1.28
14		$C_\beta H_3$	−0.12	2.41	−2.53	−2.45	−0.46	−2.91
g	Leu F4	$C_\gamma H$	*i*	0.63		4.44	−0.36	4.08
i		$C_{\delta 1}H_3$	*i*	0.44		1.20	0.25	1.45
15		$C_{\delta 2}H_3$	8.71	0.31	8.40	9.15	0.34	9.49
r	Ser F7	$O_\gamma H$	9.71	8.17	1.54	4.38	−0.05	4.33
16	Ala F9	$C_\alpha H$	6.47	3.80	2.67	3.46	0.01	3.47
g		$C_\beta H_3$	2.66	1.12	1.54	1.68	0.02	1.70
17	His FG3	$C_\beta H$	1.32	1.89[j]	−0.57	−0.46	0.25	−0.21
18		$C_\beta H'$	−0.48	2.87[j]	−3.35	−4.35	0.59	−3.76
19		$C_\delta H$	11.07	2.34	8.73	7.26	2.38	9.64
20		$C_\epsilon H$	6.83	7.91	−1.08	−2.17	1.07	−1.10
i		$N_\epsilon H$	*i*	7.98		−1.36	1.74	0.38
21	Ile FG5	$C_\alpha H$	2.35	4.29[j]	−1.94	−1.48	−0.62	−2.10
22		$C_\beta H$	−0.13	1.13[j]	−1.26	−0.09	−1.01	−1.10
23		$C_\gamma H$	−9.60	−0.28[j]	−9.32	−6.26	−3.31	−9.57
24		$C_\gamma H'$	−1.91	0.85[j]	−2.76	−1.13	−0.93	−2.06
25		$C_\gamma H_3$	−3.46	1.36[j]	−4.82	−3.16	−1.46	−4.62
26		$C_\delta H_3$	−3.83	1.47[j]	−5.30	−4.31	−1.01	−5.32
27	Leu G5	$C_\gamma H$	0.07	1.81[j]	−1.74	−1.35	−0.43	−1.78
28		$C_{\delta 2}H_3$	−1.49	1.23[j]	−2.72	−2.15	0.06	−2.09
29	Ile G8	$C_\gamma H_3$	0.37	1.80[j]	−1.43	−2.70	0.64	−2.06
i		$C_\delta H_3$	*i*	0.31		−1.16	1.09	−0.07
30	Phe H15	$C_\delta Hs$	7.02	7.08	−0.06	−0.36	0.28	−0.08[p]
31		$C_\epsilon Hs$	6.94	7.15	−0.21	−0.67	0.55	−0.12[p]
32		$C_\zeta H$	7.02	7.00	0.02	−0.52	1.01	0.48
33	Tyr H23	$C_\epsilon Hs$	7.45	6.42	1.03	1.25	−0.15	1.10[q]
h		$C_\delta H$	7.20 (?) or 7.00 (?)	6.61	0.59 or 0.39	0.73	−0.07	0.66[q]
34	Val E11	$C_\alpha H$	−2.55	3.24	−5.74	−5.15	−1.00	−6.15
35		$C_\beta H$	1.47	0.84	0.63	1.58	0.02	1.60
36		$C_{\gamma 1}H_3$	−1.02	−0.55	−0.47	−2.73	1.75	−0.98
37		$C_{\gamma 2}H_3$	−0.89	−2.30	1.41	7.17	−1.25	5.92
38	His E7	$C_\beta H$	3.81	3.08[j]	0.73	1.69	−0.08	1.61
39		$C_\beta H'$	4.41	2.72[j]	1.69	3.05	−0.09	2.96
40		$C_\delta H$	11.71	4.97[j]	6.74	10.03	0.01	10.31
41		$N_\epsilon H$	23.67	3.88[j]	19.79	24.49	1.10	25.59
i		$C_\epsilon H$	*i*	7.17		−3.94	−0.72	−4.66

[a] Shifts in ppm at 25 °C for sperm whale metMbCN in ^2H_2O or ^1H_2O (for exchangeable protons) at pH* 8.6. [b] Numbered data points have variable temperature slopes available and served as input data in the determination of $R(\alpha,\beta,\gamma)$. [c] Observed shift referred to DSS. [d] Diamagnetic shift obtained from published MbCO data (Dalvit & Wright, 1987), unless noted otherwise. [e] Observed dipolar shift obtained from eqs 1 and 4 with $\delta_{con} = 0$. [f] Dipolar shift calculated with eq 3 with $R(0°,-14.5°,35°)$ using the MbCO crystal coordinates; the axial and rhombic terms correspond to the first and second terms of eq 3. [g] Unambiguously assigned peak not used as input data in search for magnetic axes. [h] (?) designates possible assignment addressed in the text (Emerson & La Mar, 1990). [i] Not assigned to date. [j] Diamagnetic shift calculated via eq 5. [k] Individual δ_{dip}(calc) H_δs at 0.60 and 1.08 ppm, H_ϵs at 1.41 and 2.03 ppm. [m] Individual δ_{dip}(calc) H_δs at 0.71 and 2.44 ppm, H_ϵs at 1.04 and 14.24 ppm. [n] Individual δ_{dip}(calc) H_δs at 0.88 and 2.66 ppm, H_ϵs at 0.98 and 3.91 ppm. [p] Individual δ_{dip}(calc) H_δs at −0.30 and 0.14 ppm, H_ϵs at −0.50 and 0.35 ppm. [q] Individual δ_{dip}(calc) H_δs at 0.25 and 1.07 ppm, H_ϵs at 0.11 and 2.09 ppm. [r] Assignment taken from Lecomte and La Mar (1986).

dinates of the susceptibility tensor, χ. The angle α is the first rotation about the old z' axis, β is the subsequent rotation of the x–z plane about the new y axis, and γ is the final rotation of the x–y plane about the z axis that converts x',y',z' (crystal pseudosymmetry axes) in Figure 1 to x,y,z (magnetic axes).

Calculations of dipolar shifts were carried out by using the X-ray crystal structure of sperm whale MbCO (Kuriyan et al., 1986) and, in some cases, MbO_2 (Phillips, 1980). Proton coordinates were generated from the heavy atom positions by using programs BIGCHEMIO and FIXHYDRO obtained from the University of California, San Francisco, Computer Graphics Laboratory. These calculations were performed on a Vax-11750 mainframe computer. The X-ray coordinates were transferred to a μ-Vaxstation II where the rest of the manipulations of the coordinates took place. The unit cell coordinates were converted into iron-centered heme pseudosymmetry coordinates (x',y',z' in Figure 2B,C) by the SMAX program. Ring current shifts were provided by the SHIFTS program written by Dr. Keith Cross (Cross & Wright, 1985). The symmetry coordinates of assigned protons, along with their δ_{dip}(obs) values, served as input for the program GLOBMIN, which was used to search for the Euler angles that minimize

the error function F defined above. The angles were incremented in 0.5° (β) and 5° (α, γ) intervals over a complete sphere. The global minima were determined by using a variety of input data (see below). Calculation of dipolar shifts from specifically chosen Euler angles is the function of the program CALPS. The programs SMAX, GLOBMIN, and CALPS were written for the μ-Vaxstation II. Calculated and observed dipolar shifts for metMbCN refer to their values at 298 K. The calculations described above gave very similar quality fits (as judged by F/n) for both MbCO and MbO_2 structures (Kuriyan et al., 1986; Phillips, 1980), although the individual deviations did not necessarily follow the same pattern. The only really appropriate coordinates for this analysis, those from a metMbCN crystal structure, are not available. We report here only the results of calculations that use the most likely related MbCO X-ray structure.

Temperature Dependence of Dipolar Shifts. The temperature dependence of dipolar shifts is due to χ and can be represented by (Kurland & McGarvey, 1970; Jesson, 1973)

$$\chi_{ii}(T) = \chi_{ii}^{298} f(T) \tag{9}$$

where χ_{ii}^{298} are the 25 °C components of the susceptibility tensor, χ, and $f(T)$ is the temperature function normalized to unity at 25 °C. The slope for a Curie plot is given by

$$\frac{\Delta\delta_{dip}}{\Delta(1/T)} = \delta_{dip}^{298}\, \Delta f(T)/\Delta(1/T) \tag{10}$$

which in the case where the simple Curie law holds, $f(T) = 1/T$, shows that the slope is proportional to the observed hyperfine shift at 25 °C. In case of small deviations from Curie behavior, the experimental slope in the limited accessible temperature range will not extrapolate to the diamagnetic intercept at $T^{-1} \rightarrow 0$, but the slope, as described in eq 10, should still be proportional to the observed shift at 25 °C. Hence, a plot of the slope of the dipolar shift versus observed dipolar shift at 25 °C for a series of nonequivalent protons should yield a straight line.

Results

Determination of Magnetic Axes. A graphical representation of the influence of the tilt of the z axis from the heme normal on the error function defined in eq 8 is illustrated in Figure 4. As initially proposed and described earlier by Williams et al. (1985), F/n is computed at a series of β tilt angles, and this tilted vector is rotated about its heme normal, leading to a series of cones depicted in part A of Figure 4. The computed F/n at the angles described on these three cones are shown in part B of Figure 4. It is clear not only that F/n is large for z perpendicular to the heme but that a sharp minimum is achieved by tilting z (angle β) uniquely in the direction of δ-meso-H by 15° (i.e., $\beta = -15°$). The section of the cones for $\beta < -15°$ are not included for clarity, but they show that the minimum error function on successive cylinders rises steeply compared to that for $\beta \sim -15°$, while the minimum for each cylinder remains in the direction of δ-meso-H. The error functions were found to vary monotonically with each angle, leading to a single minimum. Thus it is clear that the F/n has a unique minimum for which the degree and direction of tilt of the z axis in the molecular axes is well-defined. The much steeper dependence of F/n on β than α,γ is due to the fact that $\Delta\chi_{ax}$ is $\sim 4\Delta\chi_{rh}$ (Horrocks & Greenberg, 1973). The resulting least-squares fit in smaller increments of β (0.5°) leads to the magnetic axes that can be depicted as in Figure 2, parts B (face-on) and C (edge-on). In this figure, the projection of z on the old x',y' plane (heme) defines α and the

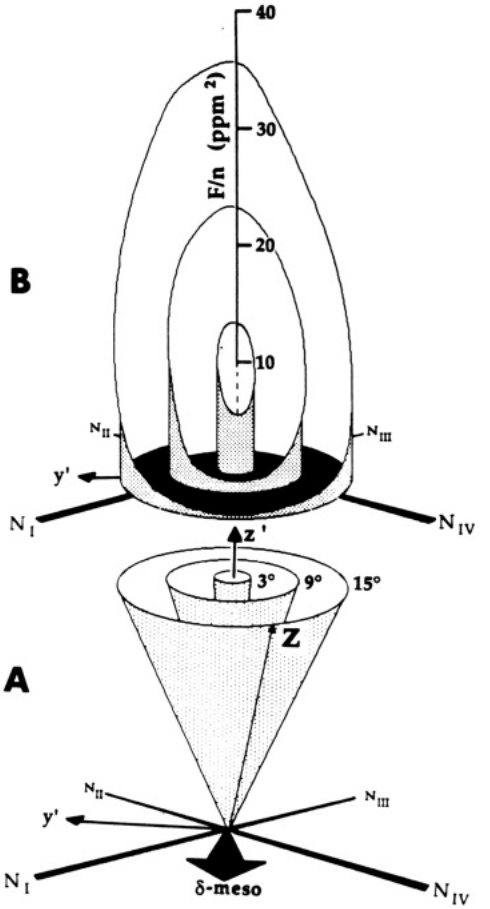

FIGURE 4: Schematic representation of the error function $(1/n)F(\alpha,\beta,\gamma)$, as a function of the tilt angle β of the z axis of the susceptibility tensor from the heme normal. The z axis is tilted in 3° increments and rotated about the z axis to form a series of cones as depicted in (A). The computed F/n is plotted for these 3° intervals of β as the fixed tilt is rotated about the heme normal as shown in (B), yielding cylinders whose heights represent the value of F/n. It is clear that F/n drops dramatically as the z axis is tilted from the heme normal in the direction of the δ-meso position. The global minimum on the cylinders occurs at $\beta \sim -15°$, with the successive cylinder for $\beta < -15°$ (not shown) rising again steeply. This useful convention for illustrating the error surface was established by Williams et al. (1985).

tilt of the z axis from the heme normal is β. For small β, the angle κ, between the projection of the new x,y axes on the heme plane and the molecular x',y' axes, can be approximated by $\kappa = \alpha + \gamma$ and defines the location of the in-plane magnetic axes.

The least-squares fits to determine $R(\alpha,\beta,\gamma)$ were carried out for four different sets of input data, in which either all 41 data points in Table I (numbered 1–41) were utilized or the shifts for His E7 of Val E11, or both His E7 and Val E11, were omitted from the input data. The orientations of the magnetic axes for these four permutations of data differed inconsequently, and the resulting values for α,β,γ and $\kappa = \alpha + \gamma$, as well as the normalized residual error function, are listed in Table II. Also included in the table are the same parameters obtained by computing F/n for the previously proposed low-temperature magnetic axes of Hori (1971) and Peisach et al. (1971). The δ_{dip}(calc) values based on the various magnetic coordinate systems listed in Table II are plotted in Figure 3 versus the δ_{dip}(obs) obtained from eq 5 ($\delta_{con} = 0$ for noncoordinated residues). A perfect fit would have all data points on a straight line with unit slope, which is shown as a solid line in each of the six plots. The dotted lines divide each plot into four quadrants, with the upper left and lower right representing areas where both shift magnitude as well as sign

Table II: Quality of Fits of Experimental and Calculated Dipolar Shifts for Various Magnetic Coordinate Systems[a]

Figure 3 plot	input data points from Table I	Euler angles, $R(\alpha,\beta,\gamma)$ (deg)					
		α	β	γ	κ[b]	F/n (ppm^2)[c]	$\bar{\sigma}$ (ppm)[d]
A	1–41	−57.5	−13.0	44.8	−13	8.1	2.8
B	1–41	−57.5	−13.0	0.0	−57	12.0	3.5
C	1–41	0	−14.0	35	35	0.98	0.99
D	1–37	10	−15.5	20	30	0.71	0.84
E	1–33, 38–41	10	−14.5	25	35	0.71	0.84
F	1–33	0	−14.5	35	35	0.28	0.53

[a] Shifts in ppm at 25 °C; δ_{dip}(obs) were determined via eqs 1, 4, and 5 (δ_{con} = 0), and δ_{dip}(calc) was obtained via eq 3 by using MbCO crystal coordinates (Kuriyan et al., 1986), $R(\alpha,\beta,\gamma)$, and χ_{ii} of Horrocks and Greenberg (1973). [b] $\kappa \sim \alpha + \gamma$ in Figure 2B. [c] Residual error function as defined in eq 8. [d] $\bar{\sigma} = (F/n)^{1/2}$.

Table III: Separation of Contact and Dipolar Shifts for Heme and His F8

resonances		δ_{DSS}(obs)[a,b]	δ_{dia}[a,c]	δ_{hf}[a,d]	δ_{dip}(calc)[a,e]			δ_{con}[a,f]
					axial	rhombic	total	
heme	1-CH_3	18.62	3.63	14.99	−4.49	1.09	−3.41	18.40
	3-CH_3	4.76	3.79	0.97	−4.72	−0.98	−5.70	6.67
	5-CH_3	27.03	2.53	24.5	−4.32	1.00	−3.32	27.82
	8-CH_3	12.88	3.59	9.29	−4.57	−1.94	−6.51	15.80
	2-H_α	17.75	8.43	9.32	−5.45	1.84	−3.61	12.93
	2-$H_{\beta c}$	−1.73	5.69	−7.42	−2.92	1.12	−1.80	−5.62
	2-$H_{\beta t}$	−2.55	5.73	−8.28	−4.54	1.73	−2.81	−5.47
	4-H_α	5.5	8.62	−3.12	−4.52	−1.72	−6.24	3.12
	4-$H_{\beta c}$	−1.95	6.29	−8.24	−1.65	−0.90	−2.55	−5.69
	4-$H_{\beta t}$	−0.77	6.61	−7.38	−2.35	−1.25	−3.60	−3.78
	α-meso-H	4.4	9.92	−5.52	−14.87	1.84	−13.03	7.51
	β-meso-H	2.09	9.34	−7.25	−10.18	−1.55	11.73	4.48
	γ-meso-H	5.98	10.15	−4.17	−12.99	1.94	−11.05	6.88
	δ-meso-H	4.09	9.86	−5.77	−11.84	−1.95	−13.79	8.02
	6-H_α	9.18	4.21	4.97	−4.37	1.79	−2.58	7.55
	6-H'_α	7.35	4.21	3.14	−6.08	2.18	−3.90	7.04
	7-H_α	1.13	4.21	−3.08	−4.72	−1.30	−6.02	2.94
	7-H'_α	−0.45	4.21	−4.66	−6.25	−0.54	−6.79	2.13
His F8/93	N_pH	13.2	7.15	6.05	5.91	0.07	5.98	0.07
	$C_\alpha H$	7.51	2.90	4.61	5.28	0.07	5.35	−0.74
	$C_\beta H$	6.43	1.72	4.71	8.06	−0.21	7.85	−3.14
	$C_\beta H'$	11.68	1.55	10.13	6.06	−0.78	5.28	4.85
	$C_\delta H$	−4.7	1.13	−5.83	7.78	−7.39	0.39	−6.22
	$N_\delta H$	20.11	9.36	10.75	16.24	0.07	16.32	−5.57
	$C_\epsilon H$	19.2	1.66	17.54	35.73	−2.41	33.32	−15.78

[a] Shifts in ppm at 25 °C for sperm whale metMbCN at pH 8.6. [b] Observed shifts referenced to DSS. [c] Diamagnetic shift obtained from MbCO (Dalvit & Wright, 1987). [d] Hyperfine shift obtained via eq 4. [e] Dipolar shift calculated via eq 3 and R(0°,−14.5°,35°). [f] Contact shift calculated via eq 1.

are predicted incorrectly. As indicated above, these plots for the previously proposed low-temperature magnetic axes (Hori, 1971; Peisach et al., 1971) yield poor fits with numerous shift directions incorrectly predicted (Figure 3A,B).

While all four considered sets of input data for the least-squares fit to determine $R(\alpha,\beta,\gamma)$ resulted in magnetic axes for which the δ_{dip}(obs) very closely correlate with δ_{dip}(calc), the quality of the fit depends somewhat on the selection of the input data (Figure 3C–F). Thus, upon including all 41 numbered data points from Table I, a good correlation is obtained with F/n = 0.98 ppm^2 (Figure 3C). It is noted, however, that the data points appear to reflect a systematic deviation in that they cluster about an apparent line with slightly greater than unit slope. The two sets of data points whose values and appropriateness may come into question are those of His E7 and Val E11 (see below). When either His E7 (input data points numbered 1–37 in Table I), Figure 3D, or Val E11 (input data points numbered 1–33 and 38–41 in Table I), Figure 3E, shifts are omitted from the fit, the systematic deviation is lessened, although the fits improve only marginally, with F/n = 0.71 in each case. However, *when both His E7 and Val E11 data points are omitted* (Figure 3F), *the fit improves significantly*, with F/n = 0.28. This trend in improved fits upon eliminating E7 and E11 was also observed with MbO_2 coordinates (Phillips, 1980); the best fit corresponding to Figure 2F gives the same F/n as when using MbCO (Kuriyan et al., 1986) although the predicted shifts show variations. As indicated above, the four separate least-squares determinations of the magnetic axes yield essentially the same values for β and $\kappa = \alpha + \gamma$, as summarized in Table II.

Using the optimal magnetic coordinate system (α = 0, β = −14.5, γ = 35), we compute δ_{dip}(calc) for all heme core substituents and the protons of the axially coordinated His F8 using eq 5. The δ_{dip}(calc), in conjunction with eqs 1 and 6, yield contact shifts as listed in Table III.

Temperature Effects on Shifts. The utility of variable-temperature shifts for peak identification was explored. In all but one case, the shifts approached the diamagnetic values as the temperature is raised. However, the apparent intercepts obtained by extrapolating to T^{-1} = 0 the straight line observed for the Curie plot in the interval 273–323 K give values far from the known diamagnetic positions. In fact, plots of shift versus reciprocal temperature (not shown) yielded intercepts for low-field (or high-field) hyperfine-shifted peaks that are strongly upfield (or downfield) of the diamagnetic positions, as observed earlier for Phe CD1 of metMbCN (Emerson et al., 1988), and as expected for a temperature dependence that has a weak T^{-2} as well as the dominant T^{-1} term (Kurland & McGarvey, 1970; Jesson, 1973; Horrocks & Greenberg, 1974).

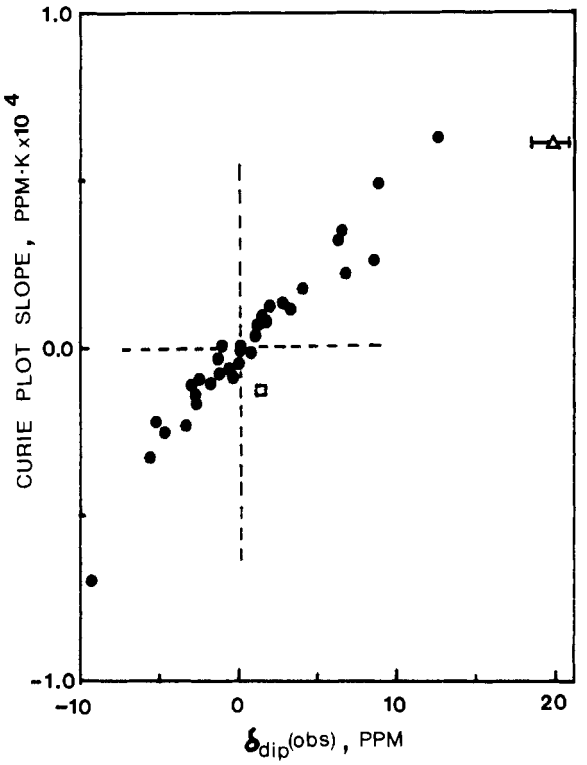

FIGURE 5: Plot of Curie slope $[\Delta\delta_{dip}(obs)/\Delta(1/T)]$ versus $\delta_{dip}(obs)$ (obtained via eqs 1 and 4 with $\delta_{con} = 0$) for assigned noncoordinated residue signals numbered 1–41 in Table I. The data points generally fall close to a straight line, as predicted by eq 10. Two data points that deviate significantly from this apparent line are Val E11 $C_{\gamma 2}H_3$ (□) (wrong sign for the slope) and His E7 $N_\epsilon H$ (△).

A plot of the experimentally observed slope in the Curie plot of the observed dipolar shift, $\Delta\delta_{dip}(obs)/\Delta(1/T)$, versus the $\delta_{dip}(obs)$ at 25 °C for the 41 numbered resonances in Table I is illustrated in Figure 5. The data points generally fall along a straight line, as would be expected if eq 10 is valid and the temperature effects for the three components of χ are very similar. This plot is again divided into four quadrants, and it is noted that only one data point, that of Val E11 $C_{\gamma 2}H_3$, falls into a (lower right) quadrant that incorrectly predicts the *sign of the slope* of the $\delta_{dip}(obs)$. The next largest deviation is for His E7 $N_\epsilon H$.[2]

Discussion

Location of the Magnetic Axes. The excellent fit between experimental and calculated dipolar shifts as found in Figure 3F demonstrates that NMR can be used to determine the magnetic axes of a low-spin hemoprotein provided the X-ray crystal coordinates of some suitable derivative, a set of ESR g values, and the unambiguous assignments of a sufficient number of heme cavity proton signals are available. The residual discrepancies probably arise from the fact that the coordinates in metMbCN are likely somewhat different from those in MbCO (Kuriyan et al., 1986). The computed χ_{ii} values also have limitations (Horrocks & Greenberg, 1973), but five-parameter optimization for the anisotropies was not deemed realistic in view of the absence of crystal coordinates for the metMbCN complex. The presently determined axes differ from those proposed earlier on the basis of single-crystal ESR spectra (Hori, 1971; Peisach et al., 1971). Since there are two slightly different magnetic axes available from such studies, it is not clear whether there is some problem with the low-temperature axes determinations, or whether the axes simply change with temperature, as previously found by ESR for both MbNO and coblat(II)-substituted MbO_2 (Hori et al., 1981, 1982).

Using the $R(\alpha,\beta,\gamma)$ for the optimal fit shown in Figure 3F, the $\delta_{dip}(calc)$ are also computed for a number of assigned residue signals in Table I for which variable-temperature data for the shifts were not available (protons of Leu B10, Ala E14, Leu F4, and Leu G5; Emerson & La Mar, 1990). It is noted that there is an excellent correlation between $\delta_{dip}(obs)$ and $\delta_{dip}(calc)$ for these protons, with the mean deviation $\bar{\sigma} = (F/n)^{1/2}$, less than for that observed from the fit (Table I). Moreover, the δ_{calc} for the three protons <7.5 Å from the iron for which we have not located the resonances place the resonances within the diamagnetic envelope, as already established (Emerson & La Mar, 1990) [$\delta_{DSS}(calc) = \delta_{dia}(calc) + \delta_{dip}(calc)$ for His FG3 $N_\epsilon H$ at ~8.26 ppm, His E7 $C_\epsilon H$ at 2.51 ppm, and Ile G8 $C_{\delta 1}H_3$ at 0.38 ppm]. More extensive 2D maps as a function of temperature may yield these desired assignments in the near future for at least the two latter nonlabile protons.

Moreover, we note that the alternate assignment in our companion report (Emerson & La Mar, 1990) of the $C_\epsilon H$ of Tyr H23 to either 7.00 or 7.20 ppm, based on COSY peaks with identical ω_2 but distinct ω_1, is readily resolved by the present study. Thus, using the $\delta_{dia}(calc)$ and $\delta_{dip}(calc)$, we find the computed δ_{dip} predicts the observed shift for Tyr H23 $C_\delta H$ at 7.2 ppm rather than 7.0. Conversely, the labile proton peaks at 9.71 ppm assigned alternately as F7 Ser γ-OH (Lecomte & La Mar, 1986) and Ala F9 peptide NH (Kumar & Kallenbach, 1985) can be predicted to exhibit a substantial downfield dipolar shift of 4.3 ppm while only a ~1.5 ppm shift is observed (Table I). While this does not confirm the assignment to Ala F8, it makes the F7 Ser γ-OH assignment very unlikely. Hence it is clear that, not only is it possible to use unambiguously assigned resonances to solve for the magnetic coordinate system, but also the predicted shifts for a reasonable orientation of the magnetic axes can be used as an aide in assignments and as a guide in the search for unassigned resonances.

Molecular Determinants of the Magnetic Axes. Taking the NMR-determined magnetic axes as shown in Figure 2B,C, with $\alpha = 0$, $\beta = -14.5$, and $\kappa = \alpha + \gamma = 35°$ as valid, we find that the projection of the rhombic magnetic axes onto the heme plane makes an angle $\kappa = 35°$ with the molecular pseudosymmetry axes that is within experimental error of the angle made by projection of the His F8 imidazole plane on the heme plane in MbCO (which is 33° for our symmetry coordinate x',y'). Thus the x axis aligns essentially parallel to the F8 imidazole plane, and it is reasonable to assume that it is precisely this iron–His F8 π bonding that determines the location of the in-plane magnetic axes. This structural basis for the determination of the rhombic axes had been anticipated earlier on the basis of the dominant heme methyl contact shift pattern (Shulman et al., 1971; Traylor & Berzinis, 1980), inasmuch as the in-plane axes and the orbital hole that causes the asymmetric contact shift pattern are related (Palmer, 1979; Byrn et al., 1983). That the z axis is tilted from the heme normal was proposed earlier by Hori (1971), but the direction of tilt was significantly different ($\alpha = -57°$, or in the direction of 2-vinyl position). In model heme complexes, the major axis of the g tensor invariably aligns with the heme normal (Palmer, 1979; Byrn et al., 1983; Inniss et al., 1988). Hence this tilt

[2] The diamagnetic chemical shift for the $N_\epsilon H$ of His E7 is not known. Due to the uncertainty in its shift arising from hydrogen-bonding effects, 9 ± 3 ppm from DSS, the resulting δ_{dip} similarly has a ±3 ppm uncertainty.

in metMbCN must reflect a protein-based deformation.

Steric interactions of distal residues with bound CO in MbCO have been proposed to provide the beneficial discrimination for a bent Fe–OO versus a perpendicular and linear Fe–CO unit (Collman et al., 1976; Dickerson & Geis, 1983), and crystal structures have indeed found the O atom of the CO well off the 4-fold axis (Norvell et al., 1975; Kuriyan, 1986). Infrared spectroscopy had revealed four CO stretches (Caughey et al., 1981), of which the dominant one has been shown to correspond to the primary CO orientation in MbCO by using polarized spectroscopy (Ormos et al., 1988; Moore, et al., 1988). Not resolved is the problem as to whether the distortion from perpendicular reflects tilting of a linear Fe–CO or a bent Fe–CO; current analysis favors a combination of effects (Li & Spiro, 1988). Several X-ray structures of metcyano complexes of various Hbs similarly propose a Fe–CN unit distorted from the pseudo-4-fold axis (Padlan & Love, 1975; Deatherage et al., 1976; Steigemann & Weber, 1979). Both the FeCO and FeCN units are linear and normal to the heme in model complexes (Peng & Ibers, 1976; Scheidt et al., 1983).

Empirical energy calculations on MbCO provide a potential energy surface for CO tilt that is consistent with the observed dominant form (Kuriyan et al., 1986). Since the FeCO and FeCN units are isostructural, and the distal residue orientations are expected to be largely conserved, we expect that the cyanide ligand would be tilted in the same direction as a carbon monoxide. The presently determined z axis of the suceptibility tensor of metMbCN is within experimental error collinear with the Fe–O vector for the primary occupation of the tilted CO in MbCO, as revealed by X-ray data (Kuriyan et al., 1986). *Thus we propose that the dominant molecular interactions that orient the susceptibility tensor are the tilt or bending of the axial cyanide ligand for the principal axis and the axial π interaction between the heme iron and the proximal histidyl imidazole for the rhombic axes.* The latter had been anticipated previously on the basis of the contact shift pattern (Shulman et al., 1971; Traylor & Berzinis, 1980); the former one has not.

Heme Electronic Structure. The factored dipolar and contact shifts for the heme core substitutents are found in Table III. The contact shifts pattern clearly reflects the asymmetric spin distribution where the e_g orbital degeneracy is lifted (Shulman et al., 1971), and the lone spin occupies the molecular orbital spanning primarily pyrroles I and III, and for these substituents δ_{dip} makes a relatively small contribution to δ_{hf}. On the other hand, for pyrrole II and IV substituents, consideration of δ_{dip} leads a δ_{con} pattern consistent with expectation for π spin density, low-field-shifted 3-CH_3, 7-α-CH_2, and alternating shift directions for H_α and H_βs for 4-vinyl (La Mar, 1973; 1979; La Mar & Walker, 1979).

Proximal His Bonding. The contact shifts resulting from factoring δ_{dip} from δ_{hf} for His F8 protons are also included in Table III. Here, because of the proximity to the iron, δ_{dip} dominates the shifts in several cases. *It was reported in our companion report that the observed shifts for His-F8 $C_\delta H$ and $C_\epsilon H$ were dramatically different from those found in the analogous model compound* (Emerson & La Mar, 1990). We note here, however, that the factored δ_{con} pattern ($C_\epsilon H$:$N_\delta H$:$C_\delta H$ ~ 3:1:1) for the imidazole side chain in metMbCN is very similar to that found upon factoring δ_{dip} and δ_{con} for the model compound (Chacko & La Mar, 1982). Thus the δ_{con} for His F8 in metMbCN does not reflect any major perturbation or strain of the protein on the Fe–His F8 bond relative to that in model compounds. It is also noted that

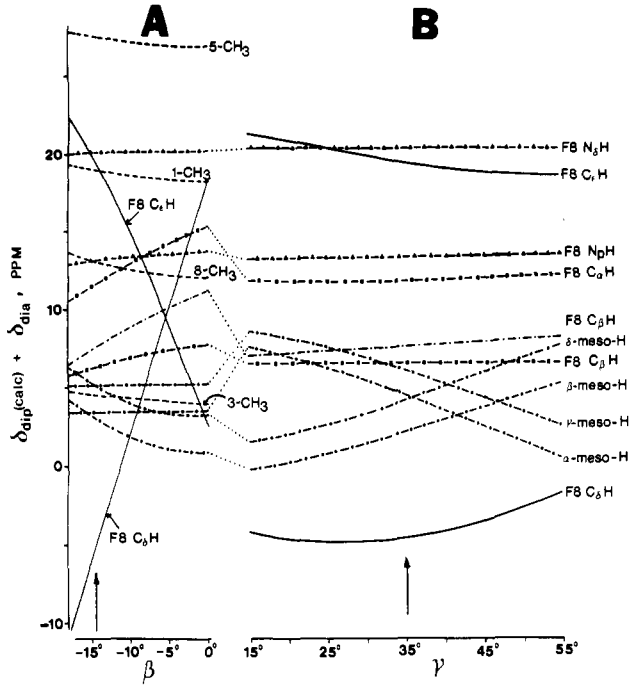

FIGURE 6: Plot of predicted chemical shifts for His F8 and selected heme positions versus systematic rotation of the magnetic axes, assuming δ_{con} and δ_{dia} are independent of the rotations, with δ_{dip}(calc) obtained from eq 5 with the selected values for the Eularian angles. (A) Variation in the tilt angle, β, of the z axis from the heme normal, keeping the orientation of the projection of the x,y (rhombic) axes in the heme plane, $\kappa = \alpha + \gamma$, constant. Notable are the extremely strong changes in shift with β, and with opposite slopes, of the two His F8 nonlabile ring protons, suggesting that the $C_\epsilon H$ and $C_\delta H$ shifts can serve as diagnostic probes of the orientation of the z axis and, hence, cyanide tilt. (B) Variation in rotation of the rhombic axes (angle γ) while keeping the degree of z-axis tilt ($\beta = -14°$) and its direction ($\alpha = 0°$) as found for the native protein. Note the only systematic variation in shift pattern is predicted for the four meso-Hs. The values of the shifts observed and predicted for the determined magnetic axes are indicated by vertical arrows.

there is a negligible δ_{con} for His F8 $N_{pep}H$, as would be expected from the distance to the iron (La Mar, 1973). The similarity of the patterns of the resulting factored His F8 ring δ_{con} and that in the model compound provides a measure of independent support for the validity of the computed δ_{dip} using the known χ_{ii} values and our NMR-determined magnetic axes.

NMR Probes of Magnetic Axes. The complete determination of the magnetic axes from a least-squares fit of a large number of experimental dipolar shifts has been demonstrated. The question is whether the results from this system provide us with readily identifiable probes of changes in the orientation of either the major axis (tilt from the heme normal) or the in-plane axes.

The fact that the δ_{hf} for the His F8 imidazole ring differs substantially in model complexes (where the z axis coincides with the heme normal) from metMbCN, in spite of establishing similar δ_{con} in both cases, dictates that the difference must originate from the magnetic axes, inasmuch as the g values and hence χ tensor are very similar (Palmer, 1979; Byrn et al., 1983; Inniss et al., 1988). Hence we compute δ_{hf} at variable z-axis tilt angle, β (keeping $\kappa = \alpha + \gamma$ invariant), and assuming δ_{con} does not change with the tilt. (In fact δ_{con} should change approximately proportional to the overlap of the imidazole and appropriate d orbitals; this should vary ~$\cos^2 \beta$ ~ 0.93 for $\beta = 15°$.) A similar calculation of δ_{hf} for heme meso-H and methyl resonances is made, keeping δ_{con} constant at the values listed in Table III. The resulting $\delta_{dip} + \delta_{dia}$ for both the heme and His F8 resonances are plotted in part A

of Figure 6; the experimentally observed values at $\beta = -14.5°$ are shown by a vertical arrow. It is clear that, while some variations in shifts are observed for all resonances, it is precisely the pair of nonlabile imidazole ring protons that change most dramatically with β, with the shifts changing sign and reversing as $\beta \rightarrow 0$. At $\beta = 0$ (z axis $\sim$ heme normal), the plot predicts $\delta_{obs}(C_\delta H) \sim 18$ ppm and $\delta_{obs}(C_\epsilon H) \sim 2$ ppm. These shifts from the appropriate model compound are $\delta_{obs}(C_\delta H) \sim 14$ ppm and $\delta_{obs}(C_\epsilon H) \sim 2$ ppm (Chacko & La Mar, 1982). Thus the susceptibility tensor and determined magnetic axes correctly predict that the His F8 ring shifts, substantially different in protein and model, approach those of the model complex as $\beta \rightarrow 0$. This can be taken as strong support for the validity of our description of the hyperfine shifts and *provides us with the desired probes of the z axis (and bound cyanide) tilt: the His F8 nonlabile ring protons.* The dramatic change in these ring proton shifts is due to the fact that the z-axis tilt occurs in a plane close to that of the His F8 imidazole (Kuriyan et al., 1986) and takes the nonlabile ring protons from near the magic angle, but with net upfield dipolar shift, and moves one into the region of large downfield and the other into the region of large upfield dipolar shift, hence the opposite slopes of δ_{hf} with β in part A of Figure 6.

Thus we propose that the broad His F8 ring protons can serve as valuable qualitative probes of the degree of tilt of the magnetic z axis (and hence of the bound cyanide) from the heme normal in a series of isostructural metMbCN complexes. Preliminary ^{1}H NMR data on sperm whale point mutants and natural mammalian Mb genetic variants reveal these broad (presumably) His F8 ring signals as the most variable spectral parameters (Krishnamoorthi et al., 1984; K. Rajarathnam, G. N. La Mar, M. Chiu, and S. G. Sligar, unpublished results). A quantitative test of this hypothesis requires complete assignment of resonances in these systems; such studies are in progress. There are few solution spectroscopics probes for such bound ligand tilt. The Fe–CO and FeC–O stretching and Fe–C–O bending vibrations yield some insight into these deformations, although quantitative comparison among closely related complexes is not simple (Li & Spiro, 1988). The use of time-resolved polarized infrared spectroscopy on photodissociating CO provides a measure of the tilt angle (Moore et al., 1988); however, such studies on model compounds suggest appreciable Fe–CO tilt (Moore et al., 1987) in spite of single-crystal structures that find essentially linear Fe–CO units normal to the heme (Peng & Ibers, 1976). Hence the presently proposed His F8 ^{1}H NMR hyperfine shift pattern provides an important new additional probe for the study of such steric distortion from perpendicular ligand bonding in heme proteins.

A similar calculation of $\delta_{dip} + \delta_{dia}$ as a function of the rotation of the rhombic axes, keeping the z axis tilted at $-14.5°$ (with $\alpha = 0$), is given in part B of Figure 6. Here we include only heme meso-Hs (which have dominant dipolar shifts) inasmuch as the heme methyl contact shifts would certainly change dramatically with κ (Shulman et al., 1971). As expected from the much smaller $\Delta\chi_{rh}$ than $\Delta\chi_{ax}$, the shift changes are both much smaller and less selective than for variable z-axis tilt angle, β. The most dramatic changes are predicted for the pattern of meso-H shifts, with very similar shifts for $\kappa \sim 45°$ (axes through N–Fe–N) and large ($\sim$10 ppm) shift alternation about the heme for $\kappa \sim 0$ (axes through meso positions). Hence the meso-H dipolar shift pattern can serve as a probe for location of the rhombic axes that is complementary to that provided by the heme methyl contact shift patterns.

Distal Residue Orientational Heterogeneity/Mobility. We noted above that, although the orientation of the magnetic axes varied only inconsequently (Table II), the quality of the least-squares fit to determine the orientation (minimization of error function, eq 8) improved slightly ($F/n = 0.98 \rightarrow 0.71$) upon ignoring either the His E7 or Val E11 data points and improved significantly ($F/n = 0.27$) upon omitting both E7 and E11 experimental shifts. There are two bases for having anticipated these results. One is that it is precisely these two distal residues that modulate ligand binding whose orientations depend most critically on the exact nature of the ligand (Takano, 1977; Kuriyan et al., 1986), and an adequate X-ray crystal structure of the derivative of interest, metMbCN, is not available. In MbCO, which should be the best model for metMbCN, neutron diffraction data find the neutral His E7 side chain with the labile ring proton on N_δ (Hanson & Schoenborn, 1981), while in MbO_2 it is found on N_ϵ and hydrogen-bonded to the bound O_2 (Phillips & Schoenborn, 1981). In fact, bound cyanide seems to exhibit properties intermediate between bound CO and O_2. ^{1}H NMR relaxation and NOE studies, as well as isotope effects on the electronic structure of the heme traceable to this His E7 $N_\epsilon H$, established that His E7 H-bonds to the bound and tilted cyanide ligand (Cutnell et al., 1981; Lecomte & La Mar, 1986, 1987). Simply using the MbO_2 crystal coordinates does not improve our fit over the MbCO data, and suggests that the distal geometry is slightly different from either MbCO or MbO_2.

In principle, the determined magnetic axes and known magnetic anisotropy could be used to search for the orientations of His E7 and/or Val E7 that best reproduce both the observed (presumed) dipolar shifts and previously reported iron-induced relaxivity. However, two observations suggest that such a fit, though likely obtainable, may not have much physical significance. For one, the fact that it has been demonstrated (Lecomte & La Mar, 1987) that there is an electronic link between His E7 $N_\epsilon H$ and the heme iron makes it likely that this labile proton experiences some contact shift contribution due to it interacting via the hydrogen bond with the known spin density of the cyanide nitrogen (Morishima & Inubushi, 1978). The largest discrepancy in the fits, that for the His E7 $N_\epsilon H$ shift (Figure 3), may be due to the fact that this hyperfine shift is *not wholly dipolar in origin.* Thus it seems imprudent at this time to include the His E7 $N_\epsilon H$ in our fit. Perhaps when the remaining elusive His E7 $C_\epsilon H$ peak is located (Emerson & La Mar, 1990), such a search for a unique His E7 orientation may be practical.

While Val E11 shifts must be wholly dipolar, an attempt to use the observed shifts to obtain the orientation would have to assume that there is one dominant orientation. We have observed that a plot of the temperature gradient of observed dipolar shifts is directly proportional to the value of δ_{dip} at 25 °C, as shown by the data in Figure 5, falling on an approximately straight line. The fact that there is such a good correlation suggests that the temperature slope of the shift can provide information on the δ_{dip} and, hence, yield an estimate of δ_{dia} that can aid in identifying the likely functional group. While there are some deviations from the straight line for numerous points in Figure 5, the data point for the Val E11 $C_{\gamma 2}H_3$ peak is unique in falling into the lower right quadrant, *where the sign of the slope differs from that of the absolute value, the apparent δ_{dip} actually increasing rather than decreasing with temperature.* This could have two likely origins: either the δ_{dia} is too low-field by $\sim$2 ppm and we have incorrectly estimated the *sign* of δ_{dip} or the Val E11 exists in more than one orientation with differential dipolar shifts, and

raising the temperature increasingly populates the orientation with larger shifts. The pattern of NOEs between the individual Val E11 γ-CH_3s and heme 1-CH_3 and 8-CH_3 in metMbCN (Emerson & La Mar, 1990) does not suggest a significant change of the mean Val E11 orientation from that in MbCO (Dalvit & Wright, 1987), and hence we tentatively conclude that the anomalous temperature dependence of the Val E11 $C_{\gamma 2}H_3$ peak reflects a mobility/heterogeneity influence. There are nodes (δ_{dip} changes sign) in both the axial and rhombic dipolar shifts between $C_{\gamma 1}H_3$ and $C_{\gamma 2}H_3$ of Val E11 (see Table I), and hence the shift may be expected to change abruptly with only small changes in coordinates. A more qualitative assessment of structural details in solution would benefit enormously from the results of a high-resolution single-crystal X-ray crystallographic structure determination of sperm whale metMbCN.

In the case of the Phe CD1, we had shown earlier by 1D NOEs that the aromatic ring is undergoing rapid reorientation on the NMR time scale, but with evidence for exchange broadening of the averaged H_ϵs signal at lower temperatures (Emerson et al., 1988). The reorientation rate was determined from estimated δ_{dip}(calc) for the nonequivalent H_ϵs. We find from the present improved fit that the two H_ϵ shifts differ more than previously reported, with the two shifts at 19.35 and 8.83 ppm for a difference of 10.52 rather than the previously assumed 5.6 ppm. This alters the rate of ring orientation at 25 °C from the previously reported 0.1 MHz to 0.35 MHz. In the other averaged ring systems, the shift differences are <2.3 ppm (Phe CD4 H_ϵs) and we observed no evidence for exchange broadening.

Acknowledgments

We are indebted to Drs. J. S. de Ropp, J. T. J. Lecomte, V. Thanabal, and S. W. Unger for useful discussions and to Professor Robert Langridge and the staff of the Computer Graphics Laboratory at the University of California, San Francisco, for making available the programs.

Registry No. Fe, 7439-89-6; CN^-, 57-12-5; L-His, 71-00-1.

References

Arfkin, G. (1985) *Mathematical Methods for Physicists*, pp 199–200, Academic Press, Orlando, FL.

Bertini, I., & Luchinat, C. (1986) *NMR of Paramagnetic Molecules in Biological Systems*, pp 19–84, Benjamin Cummings Publishing Co., Menlo Park, CA.

Bundi, A., & Wüthrich, K. (1979) *Biopolymers 18*, 285–297.

Byrn, M. P., Katz, B. A., Keder, N. L., Levan, K. R., Magurany, C. J., Miller, K. M., Pritt, J. W., & Strouse, C. E. (1983) *J. Am. Chem. Soc. 105*, 4916–4922.

Caughey, W. S., Shimada, H., Choc, M. G., & Tucker, M. P. (1981) *Proc. Natl. Acad. Sci. U.S.A. 78*, 2903–2907.

Chacko, V. P., & La Mar, G. N. (1982) *J. Am. Chem. Soc. 104*, 7002–7007.

Collman, J. P., Brauman, J. I., Halbert, T. R., & Suslick, K. S. (1976) *Proc. Natl. Acad. Sci. U.S.A. 73*, 3333–3337.

Cross, K. J., & Wright, P. E. (1985) *J. Magn. Reson. 64*, 220–231.

Cutnell, J. D., La Mar, G. N., & Kong, S. B. (1981) *J. Am. Chem. Soc. 103*, 3567–3572.

Dalvit, C., & Wright, P. E. (1987) *J. Mol. Biol. 194*, 313–327.

Deatherage, J. F., Loe, R. S., Anderson, C. M., & Moffatt, K. (1976) *J. Mol. Biol. 104*, 687–706.

Dickerson, R. E., & Geis, I. (1983) *Hemoglobin, Structure, Function, Evolution and Pathology*, pp 18–63 and 146–158, Benjamin Cummings Publishing Co., Menlo Park, CA.

Emerson, S. D., & La Mar, G. N. (1990) *Biochemistry* (preceding paper in this issue).

Emerson, S. D., Lecomte, J. T. J., & La Mar, G. N. (1988) *J. Am. Chem. Soc. 110*, 4176–4182.

Hanson, J. C. & Schoenborn, B. P. (1981) *J. Mol. Biol. 153*, 117–146.

Hori, H. (1971) *Biochim. Biophys. Acta 251*, 227–235.

Hori, H., Ikeda-Saito, M., & Yonetani, T. (1981) *J. Biol. Chem. 256*, 7849–7855.

Hori, H., Ikeda-Saito, M., & Yonetani, T. (1982) *J. Biol. Chem. 257*, 3636–3642.

Horrocks, W. D., Jr. (1973) in *NMR of Paramagnetic Molecules* (La Mar, G. N., Horrocks, W. D., Jr., & Holm, R. H., Eds.) pp 127–177, Academic Press, New York.

Horrocks, W. D., Jr., & Greenberg, E. S. (1973) *Biochim. Biophys. Acta 322*, 38–44.

Horrocks, W. D., Jr., & Greenberg, E. S. (1974) *Mol. Phys. 27*, 993–999.

Inniss, D., Soltis, S. M., & Strouse, C. E. (1988) *J. Am. Chem. Soc., 110*, 5644–5650.

Jesson, J. P. (1973) in *NMR of Paramagnetic Molecules* (La Mar, G. N., Horrocks, W. D., & Holm, R. H., Eds.) pp 1–52, Academic Press, New York.

Krishnamoorthi, R., La Mar, G. N., Mizukami, H., & Romero, A. E. (1984) *J. Biol. Chem. 259*, 8826–8831.

Kumar, N. V., & Kallenbach, N. R. (1985) *Biochemistry 24*, 7658–7662.

Kuriyan, J., Wilz, S., Karplus, M., & Petsko, G. A. (1986) *J. Mol. Biol. 192*, 133–154.

Kurland, R. J., & McGarvey, B. R. (1970) *J. Magn. Reson. 2*, 286–301.

La Mar, G. N. (1973) in *NMR of Paramagnetic Molecules* (La Mar, G. N., Horrocks, W. D., Jr., & Holm, R. H., Eds.) pp 86–1578 Academic Press, New York.

La Mar, G. N. (1979) in *Biological Applications of Magnetic Resonances* (Shulman, R. G., Ed.) pp 305–343, Academic Press, New York.

La Mar, G. N., & Walker, F. A. (1979) in *The Porphyrins* (Dolphin, D., Ed.) Part IV-B, pp 61–157, Academic Press, New York.

Lecomte, J. T. J., & La Mar, G. N. (1986) *Eur. Biophys. J. 13*, 373–381.

Lecomte, J. T. J., & La Mar, G. N. (1987) *J. Am. Chem. Soc. 109*, 7219–7220.

Li, X.-Y., & Spiro, T. G. (1988) *J. Am. Chem. Soc. 110*, 6024–6033.

Mabbutt, B. C., & Wright, P. E. (1985) *Biochim. Biophys. Acta 832*, 175–185.

Moore, J. N., Hansen, P. A., & Hochstrasser, R. M. (1987) *Chem. Phys. Lett. 138*, 110–114.

Moore, J. N., Hansen, P. A., & Hochstrasser, R. M. (1988) *Proc. Natl. Acad. Sci. U.S.A. 85*, 5062–5066.

Morishima, I., & Inubushi, T. (1978) *J. Am. Chem. Soc. 100*, 3568–3574.

Norvell, J. C., Nunes, A. C., & Schoenborn, B. P. (1975) *Science 190*, 568–569.

Ormos, P., Braunstein, D., Frauenfelder, H., Hong, M. K., Lin, S.-L., Sauke, T. B., & Young, R. D. (1988) *Proc. Natl. Acad. Sci. U.S.A. 85*, 8492–8496.

Padlan, E. A., & Love, W. E. (1975) *J. Mol. Biol. 249*, 4067–4076.

Palmer, G. (1979) in *The Porphyrins* (Dolphin, D., Ed.) Part IV, pp 313–353, Academic Press, New York.

Peisach, J., Blumberg, W. E., & Wyluda, B. J. (1971) *Eur. Biophys. Congr., Proc. 1st 1*, 109–112.

Peng, S.-M., & Ibers, J. A. (1976) *J. Am. Chem. Soc. 98*, 8032-8036.
Phillips, S. E. V. (1980) *J. Mol. Biol. 142*, 531-554.
Phillips, S. E. V., & Schoenborn, B. P. (1981) *Nature 292*, 81-82.
Satterlee, J. D. (1985) *Annu. Rep. NMR Spectrosc. 17*, 80-178.
Scheidt, W. R., Ja Lee, Y., Luangdilok, W., Haller, K. J., Anzai, K., & Hatano, K. (1983) *Inorg. Chem. 22*, 1516-1522.
Shulman, R. G., Glarum, S. H., & Karplus, M. (1971) *J. Mol. Biol. 57*, 93-115.
Springer, B. A., Egeberg, K. D., Sligar, S. G., Rohlfs, R. J., Mathews, A. J., & Olson, J. S. (1989) *J. Biol. Chem. 264*, 3057-3060.
Steigemann, W., & Weber, E. (1979) *J. Mol. Biol. 127*, 309-336.
Takano, T. (1977) *J. Mol. Biol. 110*, 537-568.
Traylor, T. G., & Berzinis, A. P. (1980) *J. Am. Chem. Soc. 102*, 2844-2846.
Williams, G., Clayden, N. J., Moore, G. R., & Williams, R. J. P. (1985) *J. Mol. Biol. 183*, 447-460.
Wüthrich, K. (1970) *Struct. Bonding 8*, 53-121.
Wüthrich, K., Shulman, R. G., Yamane, T., Wyluda, B. J., Hügli, T. E., & Gurd, F. R. N. (1970) *J. Biol. Chem. 245*, 1947-1953.

Studies on the Solution Conformation of Human Thioredoxin Using Heteronuclear ^{15}N-^{1}H Nuclear Magnetic Resonance Spectroscopy†

Julie D. Forman-Kay,‡,§ Angela M. Gronenborn,*,‡ Lewis E. Kay,‡ Paul T. Wingfield,∥,⊥ and G. Marius Clore*,‡

Laboratory of Chemical Physics, Building 2, National Institute of Diabetes and Digestive and Kidney Diseases, National Institutes of Health, Bethesda, Maryland 20892, Department of Molecular Biophysics and Biochemistry, Yale University, New Haven, Connecticut 06511, and Glaxo Institute for Molecular Biology SA, 46 Route des Acacias, CH-1211 Geneva, Switzerland

Received August 2, 1989; Revised Manuscript Received September 28, 1989

ABSTRACT: The solution conformation of uniformly labeled ^{15}N human thioredoxin has been studied by two-dimensional heteronuclear ^{15}N-^{1}H nuclear magnetic resonance spectroscopy. Assignments of the ^{15}N resonances of the protein are obtained in a sequential manner using heteronuclear multiple quantum coherence (HMQC), relayed HMQC-correlated (COSY), and relayed HMQC-nuclear Overhauser (NOESY) spectroscopy. Values of the $^{3}J_{HN\alpha}$ splittings for 87 of the 105 residues of thioredoxin are extracted from a variant of the HMQC-COSY experiment, known as HMQC-*J*, and analyzed to give accurate $^{3}J_{HN\alpha}$ coupling constants. In addition, long-range $C_{\alpha}H(i)$-$^{15}N(i+1)$ scalar connectivities are identified by heteronuclear multiple bond correlation (HMBC) spectroscopy. The presence of these three-bond scalar connectivities in predominantly α-helical regions correlates well with the secondary structure determined previously from a qualitative analysis of homonuclear nuclear Overhauser data [Forman-Kay, J. D., Clore, G. M., Driscoll, P. C., Wingfield, P. T., Richards, F. M., & Gronenborn, A. M. (1989) *Biochemistry 28*, 7088-7097], suggesting that this technique may provide additional information for secondary structure determination a priori. The accuracy with which $^{3}J_{HN\alpha}$ coupling constants can be obtained from the HMQC-*J* experiment permits a more precise delineation of the beginnings and ends of secondary structural elements of human thioredoxin and of irregularities in these elements.

The application of nuclear magnetic resonance (NMR)[1] spectroscopy to the determination of three-dimensional structures of proteins in solution has advanced rapidly in the past few years [see Wüthrich (1986) and Clore and Gronenborn (1987, 1989) for reviews]. A formidable limitation, however, still exists with respect to the size of molecules to which the methodology can be applied. One avenue for resolving ambiguities in assignment arising from severe spectral overlap associated with molecules larger than ~10 kDa was opened by the development of heteronuclear ^{15}N-^{1}H experiments. In addition to the powerful three-dimensional heteronuclear experiments reported recently (Marion et al., 1989a,b; Zuiderweg & Fesik, 1989), two-dimensional heteronuclear relayed multiple quantum and multiple bond correlation experiments can also be used to deal with problems caused by overlapping resonances and confirm assignments (Gronenborn et al., 1989a,b; Clore et al., 1988). ^{15}N-^{1}H HMQC, relayed HMQC-NOESY, HMQC-COSY, and HMBC experiments have been recorded on human thioredoxin

†This work was supported by the Intramural AIDS Targeted Antiviral Program of the Office of the Director, NIH (A.M.G. and G.M.C.). J.D.F. acknowledges a graduate fellowship from the Molecular Biophysics and Biochemistry Department of Yale University and support from NIH Grant GM-22778 (to F. M. Richards, Yale University).
‡National Institutes of Health.
§Yale University.
∥Glaxo Institute for Molecular Biology SA.
⊥Present address: Protein Expression Laboratory, Building 6B, National Institutes of Health, Bethesda, MD 20892.

[1] Abbreviations: NMR, nuclear magnetic resonance; HMQC, heteronuclear multiple quantum correlation spectroscopy; NOESY, two-dimensional nuclear Overhauser effect spectroscopy; COSY, two-dimensional correlated spectroscopy; HMQC-COSY, relayed heteronuclear multiple quantum coherence correlated spectroscopy; HMQC-NOESY, relayed heteronuclear multiple quantum coherence nuclear Overhauser spectroscopy; HMBC, heteronuclear multiple bond correlation spectroscopy; NOE, nuclear Overhauser effect; *E. coli*, *Escherichia coli*; DTT, dithiothreitol.

0006-2960/90/0429-1566$02.50/0